Journal of Optoelectronic and Biomedical Materials Vol. 14, No. 4, October-December 2022, p. 203-210

Design of micro-jet plasma system: a novel nanoparticles manufacturing method in atmospheric pressure

N. Kh. Abdalameer*, S. N. Mazhir, H. M. Salim, J. Kh. Hammood, Z. H. Abdul Raheem
University of Baghdad, college of science for Women, Baghdad, Iraq, department of Physics

Micro jet atmospheric (MPJ) plasma was first utilized to create nano-sized crystals. Nano-sized particles may have advantageous characteristics such as better internal quality and dissolving rates of the product compared to traditional crystalline goods. A nebulizer system sprays an aerosol solution into plasma by use of a carrier gas in a cold plasma crystal (argon). The plasma warms and loads the droplets causing solvent and columbic fission evaporation, and then the nucleation and crystal formation start within the limited volume given by the tiny drops. This produces nano-sized crystals. MPJ was used to establish the operating parameters for producing nano-sized ZnSe material crystals using electron microscope transmitting and X-ray powder diffraction tests as well as sensitivity testing have been carried out. Sensitivity tests showed lower friction sensitivity for the nano-scale product, suggesting a better internal quality of the crystal product.

(Received July 17, 2022; Accepted November 3, 2022)

Keywords: MPJ, Cold plasma, Atmospheric plasma, ZnSe, Nano-sized crystal

1. Introduction

Since their discovery in 1968, low temperature atmospheric pressure plasmas (APP) have been used to treat a wide variety of materials[1]. The tube design is one of the most often used APP applicators and includes the plasma jet, plasma needle, plasma pencil, and micro plasma jet[2]. These tube sources' plasma operating modes are affected by their electrode design, gas flow rate, gas type, applied power, and distance between the plasma applicator nozzle and treated surface[3]. The purpose of this research is to examine the Plasma Stream, an industrial-scale low temperature atmospheric plasma jet system[4]. The primary distinction between this system and plasma needle, pencil, and micro plasma jet systems is the electrode structure[5], the increased distance between the electrode and the treated surface, and the larger nozzle area. Several uses of this source have been described to date, including increasing silicone adherence to steel[6], controlling cell adhesion, and deposition of plasma polymerized coatings[7]. These investigations indicated that factors such as the applied power and the gap distance between the substrate and the jet nozzle have a substantial effect on the coating characteristics that are deposited[8]. For example, when plasma-coated primer coatings were deposited prior to attaching siloxane elastomers to stainless steel, increasing the gap distance resulted in substantially decreased adhesive binding strengths for the primer coatings[9]. Understanding the nature of the initiating plasma, the thermal properties of the system, and the effect of operating parameters such as input power, gas flow, and the source to substrate distance on these properties is a critical first step toward determining the plasma kinetics and thus the potential range of applications of atmospheric plasma jet[10]. Nano-sized crystals may have remarkably diverse chemical and physical characteristics because the particle surface properties of the bulk dominate. Because smaller particles have a considerably larger surface area, the total dissolving rate is anticipated to rise at the same driving power for dissolution. In addition, nano-sized crystals are too tiny to include

* Corresponding author: nisreenka_phys@csw.uobaghdad.edu.iq
https://doi.org/10.15251/JOBM.2022.144.203

inclusions whose size generally fits in the micron size range. These pockets of mother liquor usually cause additional crystalline flaws, such as dislocations[11].

2. Cold plasma atmospheric pressure

Cold plasma atmospheric pressure Plasma comprises of the excited or grounded electrons, ions and neutral substances. The ionization level may describe plasma. Gas is usually completely ionized in thermal plasma and electrons and ions have an equivalent temperature[12]. If a tiny percentage of the gas is ionized and the energy electrons are too little to heat the gas, the plasma is known as non-thermal or cold plasma[10]. The ionized gas as a whole (ions and molecules) is still relatively low in cold plasma. However, the electron temperature is usually several thousand degrees since the electrons become more excited owing to their lower mass relative to the heavier ions, and thermal balance is not achieved[13]. Our study focused on the use of cold plasma.

3. Experimental setup

3.1. Designing a Micro Plasma Jet system to produce non-thermal plasma under Atmospheric pressure

The system has three parts:

1- Power supply high voltage.
2- The first electrode (stainless steel micro tube).
3- The second electrode (stainless steel sheet or metal used).
4- Argon gas.
5- Flow meter, which controls the gas flow, adjusted to 3 L/min.

3.2. High voltage power supply

A high voltage DC power supply has been manufactured to generate a high tension voltage varying from (0 to 16 kV) with low current about (1.66 mA) and the consumed power of the system about (26.48 W) to produce cold plasma, as shown in Figure (1)

3.3. Electrodes

A hollow metal tube made of stainless steel, 3 cm in length and 700 μm in diameter is the first electrode which the gas has passed through and linked to the power-supply anode terminal and positioned at 1 cm above the liquid. The second electrode is made of a metal strip of conductive stainless steel, which is 6 cm long and 5 mm wide and terminates with a flawless piece (1 pc 1) cm attached to the cathode power connector. Figure (2) illustrates the schematic micro-plasma jet diagram.

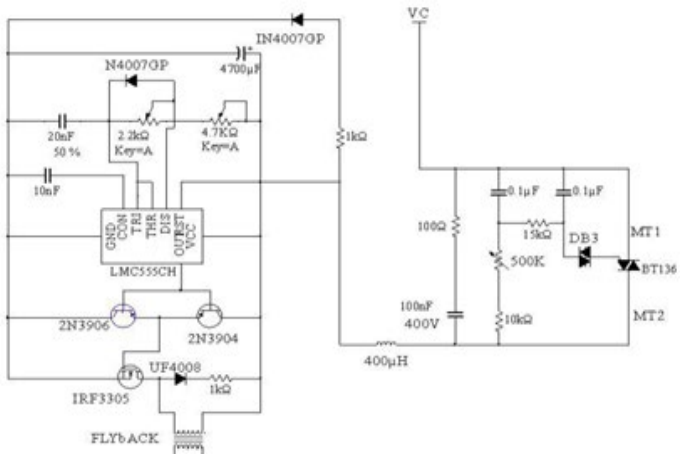

Fig. 1. Schematic diagram of high voltage (DC) power supply.

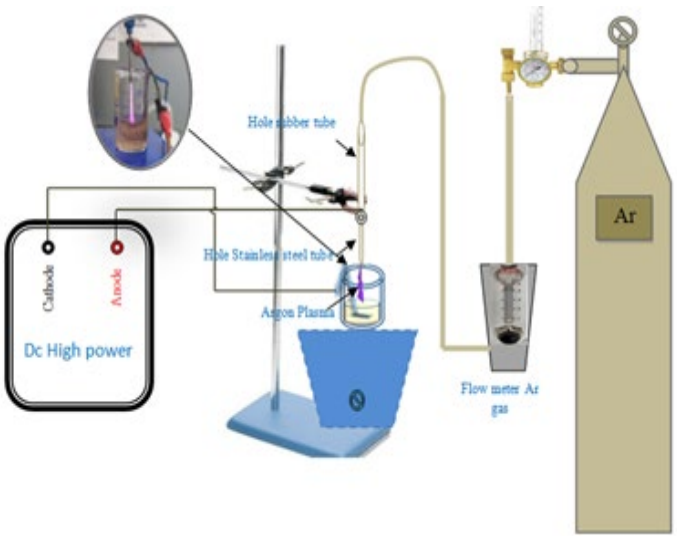

Fig. 2. Schematic diagram of micro plasma jet system.

3.4. Preparation of selenium saltsolution

Saltwater saline Selinum solution ($SeO(NO_3)_2$) was produced with a concentration of 0.1M by means of a reaction of selenium dioxide (SeO2Avonchem, UK) in just 100ml of deionized water with nitric acid (HNO3) (CDH, India) as follows:

$$SeO_2 + 2HNO_3 = SeO(NO_3)_2 + H_2O$$

2 ml produced with 500 ml deionized water, where the molecular weight was 218.96 g/mol, so that the concentration of salt solution was 0.0004 M.

3.5. Preparation of selenium NP_s and ZnSe NP_S

This method consisted of exposure to cold plasma of 10 ml of Selene nitrate at a concentration of 0.0004 molar in a 25 ml glass beaker or at a gas flow rate of 2 l/min 3 minutes. The color of the solution is observed as an indication of Nanoparticles. Then we changed the flat electrode with a zinc sheet on the pre-prepared Nanoparticles of selenium and exposed them to the plasma under the same time and gas flow conditions. We observed a change in color in the solution as an indication for the acquisition of Nanoparticles with selenium NPs at their core (see Figure3).

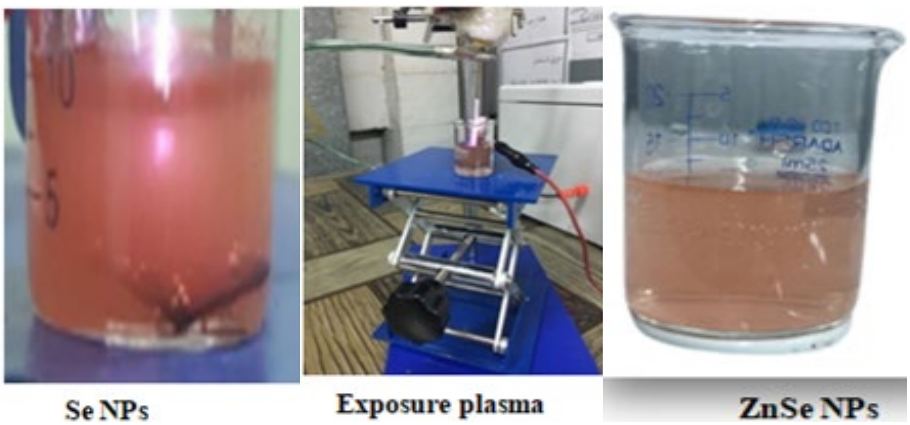

Fig. 3. Colored solution of ZnSe nanoparticles with a time of plasma exposure (3 min) and concentration 0.04 nM.

4. Results and discussion

4.1. Electrical and spectral properties of the designed micro plasma jet system.

The output high voltage was measured by a high voltage probe (SEW® PD-28) with a ratio of conversion 1:1000, for current measurements, (PROVA 15 AC/DC mA current probe) was utilized. The power supply of the system contains main switch that is used to adjustment of the power of cold plasma. Table (1) summarizes the range of output high voltage and discharges current of the power supply of micro jet plasma system. It was found that the minimum voltage that ignites the plasma about (7.32 kV) and discharge current about (0.192mA), the plasma that is generated in this region is weak. Also, the discharge current increased linearly with the output voltage, the breakdown voltage is about 15.9 kV, the value of the output current in the glow discharge region. The discharge appeared is very intense, dense, and homogenous, the output voltage started from (9-16 kV), it is fixed at the value of current ≈ 1.66mA. The cold plasma that is generated in this region was categorized by low temperature plasma (cold plasma).

4.2. Discharge Power Calculation

To determine the discharge power of Micro jet plasma system it used the product of voltage and current formula as shown in Table (2). Power and treatment time are important parameters specially, when using plasma with living tissues. The output power should not be exceed 100 W for 5 second, otherwise be harmful and caused necrosis cell.

Table 1. The electrical characteristics of micro plasma jet system.

	F=23 kHz, Flow rate = 3 l/min							
No.	1	2	3	4	5	6	7	8
V_{out} (Kv)	7.32	8.63	9.95	10.83	11.62	12.04	13.38	15.9
I_{out} (mA)	0.19	0.39	1.09	1.16	1.23	1.36	1.52	1.66

Table 2. Discharge power of system.

	F=23 kHz, Flow rate = 3 l/min							
No.	1	2	3	4	5	6	7	8
V_{out} (Kv)	7.32	8.63	9.95	10.83	11.62	12.04	13.38	15.9
I_{out} (mA)	0.19	0.39	1.09	1.16	1.23	1.36	1.52	1.66
P(W)	1.45	3.43	10.84	12.56	14.29	16.37	20.33	26.48

4.3. Energy density Calculation

As shown in Table (3). To determine the energy density of Micro jet plasma system it used the formula:

$$Energy\ density = \frac{power}{flow\ rate} \quad (1)$$

Table 3. Energy density of system.

	F=23 kHz, Flow rate = 3 l/min							
No.	1	2	3	4	5	6	7	8
P(W)	1.45	3.43	10.84	12.56	14.29	16.37	20.33	26.48
Energy density (W.min/l)	0.48	1.14	3.61	4.18	4.76	5.54	6.77	8.82

4.4. X-Ray Diffraction Investigation

The produced ZnSe Nanoparticles are displayed in the Figure (4) as X-ray diffraction patterns of non-thermal plasma. The XRD models of ZnSe, prepared by non-thermal plasma, have shown major peaks at diffraction angles (27.22, 29.25, 38.02, 45.37) and (35.28) of Zn (111), (101), (110) and (002) corresponding planes. This result agrees well with that presented in references[14]. In general, ZnSe forms in both hexagonal wurtzite structure and cubic zinc blend structure, structure which were matches well the standard peaks (JCPDS NO. 00-005-0522). From the x-ray patterns, the broadening of the diffraction peaks of the Nanoparticles is obvious, the crystallite size (D) calculated by using Scherer formula (1)[15]:

$$D = \frac{0.9\,\lambda}{\beta\,cos\theta} \tag{2}$$

The peak widths of a strong diffraction plane were calculated which they found value of D shows that the size lies within the Nanoparticles range which the average crystalline size of ZnSe NTP is (51.28)nm and listed in the table (4).

Table 4. Structural properties resulting from XRD of ZnSe NPs prepared by physical method.

Sample	FWHM (Deg.)	2 Theta(Deg.)	C.S (nm)	Avg. C.S	hkl
ZnSe	0.15	27.22	54.62	51.28	111
	0.19	29.25	43.31		101
	0.12	36.29	69.83		102
	014	37.96	60.14		110
	0.30	43.23	28.54		002 Zn

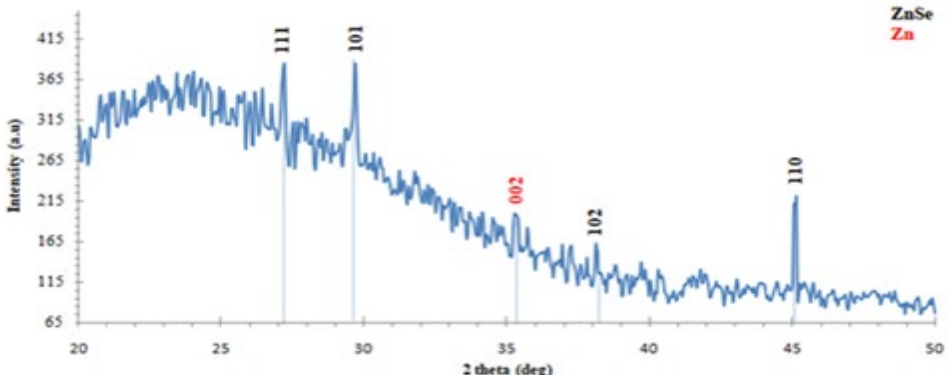

Fig. 4. Illustrates the X-ray diffraction spectrum of ZnSe prepared by non-thermal plasma (physical method).

4.5. Atomic Force Microscopy Analysis (AFM)

Three dimensional (3D) AFM profiles are used to provide materials with information on the morphology of the surface. Figures (5) demonstrate the ZnSe NPs preparation surface morphology by non-thermal plasma. Where it was noted that the average granular material diameter prepared in the green method is less than the granular diameter of the prepared substance without the extract, meaning that the extract produces a particle capping and thus the material cannot be aggregated together and thus keeps the particulate size intact. Table (5) provides physical technique AFM parameters for ZnSe NPs.

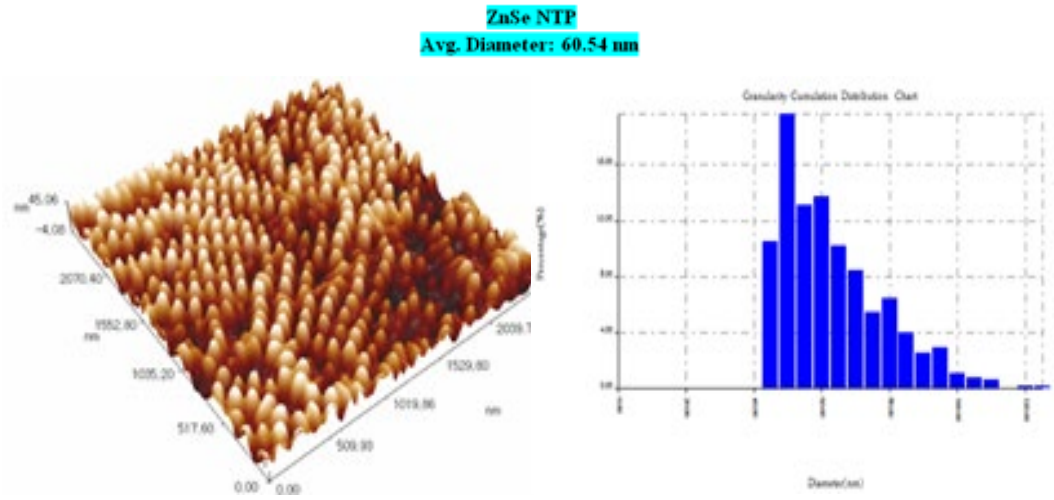

Fig. 5. 3D AFM and their granularity accumulation distribution for ZnSe NPs physical method.

Table 5. Shows the AFM parameters for ZnSe Nps by physical method.

Sample	Avg. Diameter(nm)	R.M.S (nm)	Avg. Roughness(nm)
ZnSe	60.54	5.87	6.50

4.6. Transmission Electron Microscopy (TEM)

The ZnSe produced Nanoparticles were used to analyze the size, shape and morphology of the transmission electron microscopy (TEM), as shown in figure (6). These findings demonstrate that the particles have spherical shape and are evenly distributed (mono dispersed) without major agglomerations.

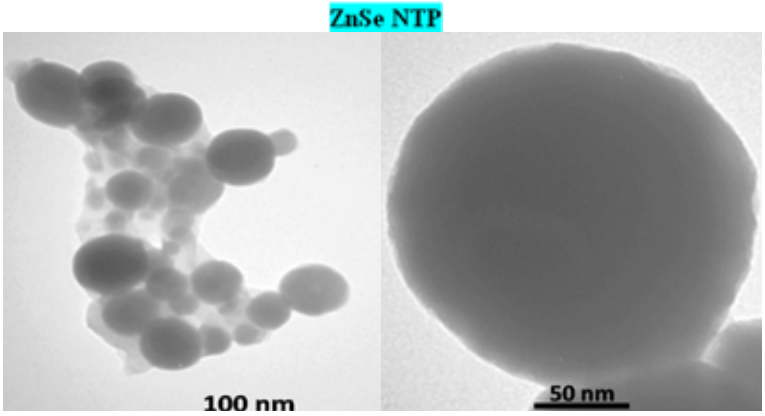

Fig. 6. TEM image of ZnSe NPs by physical method.

4.7. Optical Energy Band Gap (E_g)

The band gap energy can be obtained in nanomaterials from maximum absorption. According to the theory of quantum confinement, the electrons in the conductivity band, and the holes in the valence band are spatially confined to the potential barrier of the surface. Due to confinement of both electrons and holes, the lowest optical transmission of energy from the valence to the conduction band increases the energy, effectively increasing the band gap (Eg)[16].

A shoulder or peak spectrum corresponds to the fundamental absorption edges of samples; the optical energy band gap for ZnSe Nanoparticles has been calculated using absorption edge. The bulk ZnSe exhibit a narrow band gap of about 2.7 eV, while in this study the showed a very large energy gap as show in table (6) increasing the band gap energies of ZnSe nanostructure could be an indication of the quantum confinement effect due to decreasing size of structure. These results have good agreement with the results obtained from XRD, AFM, and TEM measurements. Figure (7) show the UV-VIS absorption spectra of the ZnSe NPs have been recorded, to measure their band - gap.

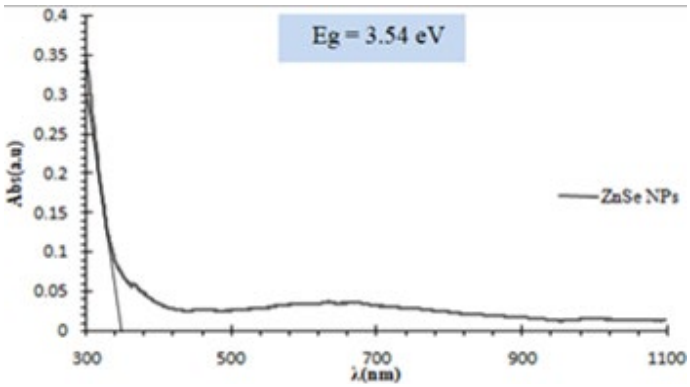

Fig. 7. UV-Vis absorbance spectra of ZnSe NPs prepared by physical method.

Table 6. Band gaps from UV-Vis absorption spectra of the samples.

Manufacturing method	Absorption wave length(nm)	Band gap (eV)
Physical	350	3.54

5. Conclusions

Atmospheric pressure argon plasma jets were manufactured and characterized by a low frequency pulsed dipole source. A range of options were taken to establish optimum conditions ideally suited to material processing or biological applications including electrode material and operating parameters and to characterize plasma jets.

We made ZnSe core-shell NPs using cold plasma with zinc plate and selenium nitrate. We have adjusted optical characteristics to the required ZnSe-NP particle size to enhance the absorption coefficient affecting the solar cell's efficiency. The absorption peaks of all nanoparticles were shown by their quantum containment in their optical spectrum. This technique offers numerous cost, speed, and repeatability benefits.

References

[1] N. K. Kaushik et al., Nanomaterials, vol. 9, no. 1, pp. 1-19, 2019; https://doi.org/10.3390/nano9010098

[2] Y. H. Usta, E. Çukur, Ç. Yıldırım, and U. K. Ercan, J. Electrostat., vol. 99, no. September 2018, pp. 1-8, 2019; https://doi.org/10.1016/j.elstat.2019.03.002

[3] C. Varilla, M. Marcone, and G. A. Annor, Foods, vol. 9, no. 10, pp. 1-17, 2020; https://doi.org/10.3390/foods9101435

[4] W. H. Chiang, D. Mariotti, R. M. Sankaran, J. G. Eden, and K. Ostrikov, Adv. Mater., vol. 32,

no. 18, 2020; https://doi.org/10.1002/adma.201905508
[5] K. Kitano, S. Hamaguchi, and H. Aoki, "Low-temperature non-thermal micro plasma jets for chemical reactions in liquids," Ispc_18, pp. 2-5, 2007.
[6] Y. Guan, G. Zhao, and X. Xiao, Propuls. Power Res., vol. 2, no. 3, pp. 188-193, 2013; https://doi.org/10.1016/j.jppr.2013.07.005
[7] S. N. Mazhir, N. H. Harb, N. A. Abdullah, N. K. Abdalameer, and H. I. Al-Ahmed, Baghdad Sci. J., vol. 15, no. 2, pp. 205–210, 2018, http://dx.doi.org/10.21123/bsj.2018.15.2.0205
[8] A. A. R. Niema, E. M. Abbas and N. K. Abdalameer, Digest J. Nanomater. Biostruct. 16, 1479 (2021).
[9] N. K. Abdulameer, Impact of Dielectric Barrier Discharge (DBD) Plasma on the Optical Properties of Thin Films, vol. 15, no. 8, pp. 1937-1942, 2020.
[10] N. Kh, K. A. Khalaph, and E. M. Ali, Mater. Today Proc., vol. 45, pp. 5788–5792, 2021, https://doi.org/10.1016/j.matpr.2021.03.166
[11] N. Radacsi, A. E. D. M. Van Der Heijden, A. I. Stankiewicz, and J. H. Ter Horst, J. Nanoparticle Res., vol. 15, no. 2, 2013; https://doi.org/10.1007/s11051-013-1445-4
[12] Razuqi, Nada S., et al. Annual Research & Review in Biology (2017): 1-9; https://doi.org/10.9734/ARRB/2017/34642
[13] T. Maho, X. Damany, S. Dozias, J.-M. Pouvesle, and E. Robert, Clin. Plasma Med., vol. 9, pp. 3-4, 2018; https://doi.org/10.1016/j.cpme.2017.12.005
[14] R. Indirajith, M. Rajalakshmi, K. Ramamurthi, M. B. Ahamed, and R. Gopalakrishnan, Ferroelectrics, vol. 467, no. 1, pp. 13-21, 2014; https://doi.org/10.1080/00150193.2014.874892
[15] N. K. Abdalameer, S. N. Mazhir, and K. A. Aadim, Energy Reports, vol. 6, no. April, pp. 447-458, 2020; https://doi.org/10.1016/j.egyr.2020.09.023
[16] Z. J. Shanan, N. K. Abdalameer, and H. M. J. Ali, *Int. J. Nanosci.*, vol. 21, no. 3, pp. 1–6, 2022; https://doi.org/10.1142/S0219581X2250017X

.